

# Bulk motion Comptonization in black-hole accretion flows

Andrzej Niedźwiecki<sup>1\*</sup> and Andrzej A. Zdziarski<sup>2\*</sup>

<sup>1</sup>*Lódź University, Department of Physics, Pomorska 149/153, 90-236 Lódź, Poland*

<sup>2</sup>*Centrum Astronomiczne im. M. Kopernika, Bartycka 18, 00-716 Warszawa, Poland*

Accepted 2005 October 18. Received 2005 October 11; in original form 2005 July 22

## ABSTRACT

We study spectra generated by Comptonization of soft photons by cold electrons radially free-falling onto a black hole. We use a Monte Carlo method involving a fully relativistic description of Comptonization in the Kerr space-time. In agreement with previous studies, we find that Comptonization on the bulk motion of free fall gives rise to power-law spectra with the photon index of  $\Gamma \gtrsim 3$ . In contrast to some previous studies, we find that these power-law spectra extend only to energies  $\ll m_e c^2$ . We indicate several effects resulting in generic cutoffs of such spectra at several tens of keV, regardless of any specific values of physical parameters in the model. This inefficiency of producing photons with energies  $\gtrsim 100$  keV rules out bulk motion Comptonization as a main radiative process in soft spectral states of black-hole binaries. The normalization of the power law (below the cutoff) with respect to the peak of the blackbody emission of the surrounding disc is typically very low, except for models with an overlap between the disc and the plasma, in which case the spectra are very soft,  $\Gamma \gtrsim 4$ .

**Key words:** accretion, accretion discs – binaries: general – black hole physics – radiation mechanisms: non-thermal – X-rays: stars.

## 1 INTRODUCTION

Bulk motion Comptonization (BMC) was first considered in a series of papers by Blandford & Payne (1981a, b) and Payne & Blandford (1981). They derived the transfer equation in the diffusion approximation for photons repeatedly upscattered by cold electrons undergoing converging inflow. Refining that approach, Psaltis & Lamb (1997) introduced relativistic corrections to that transfer equation, solved by Psaltis (2001) in a flat spacetime. Solution of the transfer equation yields a power-law spectrum with a photon spectral index of  $\Gamma = 3$  for the velocity profile corresponding to free fall. Titarchuk & Zannias (1998) and Turolla, Zane & Titarchuk (2002) showed that this property remains valid when effects of general relativity are taken into account. While the above studies demonstrate the ability of this model for producing power-law spectra by scattering on the bulk motion, they do not determine how far such a spectrum extends to high energies. In particular, the Compton recoil and other effects resulting in high energy turnover of the spectrum were not taken into account in those papers.

Notwithstanding the uncertainty about that issue, Chakrabarti & Titarchuk (1995) and Ebisawa, Titarchuk & Chakrabarti (1996) proposed the BMC to be responsible for producing high-energy tails in the soft spectral states

of black-hole binaries. They argued that both Keplerian and sub-Keplerian (close to free fall) components are always present in black-hole accretion flows. In the hard state, the latter is hot, and thermal Comptonization dominates. In the soft state, the sub-Keplerian flow remains cold and Comptonization on the bulk motion explains the presence of high-energy tails, which are observed to have typically  $\Gamma \simeq 2.5$ – $3.5$ . Then, application of their BMC model to observational data of several sources was presented by, e.g., Shrader & Titarchuk (1998, 1999) and Borozdin et al. (1999).

On the other hand, e.g., Zdziarski (2000), Zdziarski et al. (2001), McConnell et al. (2002) and Zdziarski & Gierliński (2004) pointed out that the high-energy tails observed in the soft states of black hole binaries extend to energies well above  $\sim 0.5$  MeV (see also Grove et al. 1998; Tomsick et al. 1999; Ueda et al. 2002), without showing any signature of a high-energy cutoff. In particular, the high-energy tail of the black-hole binary Cyg X-1 in the soft state shows no cutoff up to 10 MeV (McConnell et al. 2002).

Another disagreements between theoretical predictions of the BMC model and observational data, noted by Zdziarski (2000), concerns Compton reflection (e.g., Magdziarz & Zdziarski 1995) which is strong in the soft state of black-hole binaries (e.g., Gierliński et al. 1999), while it should be close to null according to the BMC model. Furthermore, the presence of the tail in the soft state was claimed to be a unique black hole signature as the BMC

\* E-mail: amn@kfd2.fic.uni.lodz.pl, aaz@camk.edu.pl

process requires the presence of a horizon (e.g., Laurent & Titarchuk 1999, hereafter LT99). However, by now, observations of weakly-magnetized accreting neutron-star binaries in the soft state show high energy tails to be common (e.g., Di Salvo et al. 2000, 2001, 2002; D’Amico et al. 2001; Iaria et al. 2001; Farinelli et al. 2005).

Still, the cutoff energy seems to be a key feature allowing to test the model against data. However, its determination has remained relatively uncertain. The studies dealing with the position of the high energy cutoff include an approximate analytic analysis in Titarchuk, Mastichiadis & Kylafis (1997) and Monte Carlo simulations by LT99 and Laurent & Titarchuk (2001). The Monte Carlo calculations of LT99 have been then compared with the *CGRO/OSSE* soft-state spectra of the black-hole binaries GRO J1655–40 and GRS 1915+105 by Zdziarski (2000) and Zdziarski et al. (2001), respectively, showing that the BMC predicted spectra fall below of the observed ones at energies  $\gtrsim 100$  keV.

Titarchuk et al. (1997) have presented a simple formula for the cutoff energy derived under the assumption that the cutoff occurs at the energy for which energy gains are balanced by energy losses in the plasma rest frame, but ignoring light bending as well as photon trapping. We find that their formula significantly overestimates the cutoff energy even if these effects are not important. LT99 use a fully relativistic description of photon propagation and scattering in the Schwarzschild metric. However, their model appears to oversimplify the treatment of photon transfer in an accreting plasma, as we discuss in Section 2.

In this paper, we study formation of BMC spectra using a Monte Carlo method described in Niedźwiecki (2005, hereafter N05) in a model with radially free-falling electrons in a plasma around a black hole. The plasma Comptonizes seed photons from an optically-thick disc. Our model involves a fully general relativistic (GR) description of photon transfer and Compton scatterings in a plasma located close to a Kerr black hole. In addition, for illustrative purposes, we calculate spectra from a model with photon trajectories approximated by straight lines.

## 2 THE MODELS

We consider a black hole accreting matter at a mass accretion rate,  $\dot{M}$ . The black hole is characterized by its mass,  $M$ , and angular momentum,  $J$ . In our model we use three reference frames. Photon trajectories are described in the Boyer-Lindquist coordinate system,  $x^i = (t, R, \theta, \phi)$  (which generalizes the Schwarzschild coordinate system for  $J \neq 0$ ). Physical processes (in particular Compton scattering) are described in local rest frames of the matter. Finally, reference frames of the locally non-rotating observers (observers with constant  $r$  and  $\theta$  but dragged in the azimuthal direction; in the Schwarzschild metric they are equivalent to static observers, i.e., observers with  $r, \theta, \phi = \text{const}$ ), introduced by Bardeen, Press & Teukolsky (1972), are auxiliary in our model. We use the following dimensionless parameters:

$$r = \frac{R}{R_g}, \quad \hat{t} = \frac{ct}{R_g}, \quad \hat{m} = \frac{\dot{M}}{\dot{M}_E}, \quad a = \frac{J}{cR_g M}, \quad (1)$$

where  $\dot{M}_E = 4\pi GMm_p/(\sigma_T c)$  is the Eddington accretion rate and  $R_g = GM/c^2$  is the gravitational radius. The formalism used by us does not work for  $a = 0$  (specifically, the turning point in  $\theta$ -motion is found according to the formalism described in Chandrasekhar 1983, which requires  $a \neq 0$ ); therefore, spectra for a non-rotating black hole are obtained assuming  $a = 10^{-3}$ .

For most of spectra presented in this paper, we assume that a Keplerian, optically thick, disc is replaced by a free-falling plasma within  $r_{\text{tr}}$ . We assume  $r_{\text{tr}} = 20$ , for which a relatively high fraction of disc photons is scattered by the plasma. The plasma is assumed to be spherical, neglecting its likely flattening. Both these assumptions maximize the importance of the BMC for spectral formation. In Section 3.6, we consider also a model where the disc (surrounded by the free-falling plasma) extends down to the event horizon.

Velocity field of the free-fall, with null angular momentum, is given by

$$u^t = \frac{A}{\Sigma\Delta}, \quad u^r = -\frac{(A - \Delta\Sigma)^{1/2}}{\Sigma}, \quad u^\theta = 0, \quad u^\phi = \frac{2ar}{\Sigma\Delta}, \quad (2)$$

where

$$\Delta = r^2 - 2r + a^2, \quad \Sigma = r^2 + a^2 \cos^2 \theta, \\ A = (r^2 + a^2)^2 - a^2 \Delta \sin^2 \theta, \quad (3)$$

yielding the velocity in the locally non-rotating frame,

$$\beta^r \equiv \frac{v^r}{c} = \frac{A^{1/2} u^r}{\Delta u^t}, \quad v^\theta = 0, \quad v^\phi = 0, \quad (4)$$

with the corresponding Lorentz factor,  $\gamma = [1 - (\beta^r)^2]^{-1/2}$ .

We assume that the rest density of electrons,  $n$ , is uniform on surfaces of constant  $r$ , and determine the density radial profile from the continuity equation. Assuming a pure H plasma, where the comoving mass density is  $\rho = nm_p$ , and integrating the mass conservation equation, we obtain,

$$n(r) = \frac{2\hat{m}}{R_g \sigma_T \int_0^\pi |g|^{1/2} |u^r| d\theta}, \quad (5)$$

where  $g$  is the determinant of the metric,  $|g| = \Sigma^2 \sin^2 \theta$ . Below we also use a dimensionless density parameter,

$$\hat{n} \equiv n R_g \sigma_T. \quad (6)$$

For  $a = 0$ , equations (4) and (5) yield  $\beta^r = -(2/r)^{1/2}$  and  $\hat{n} = (2/r)^{1/2} \hat{m}/2r$ , respectively, and for  $a = 0.998$ , departures from these profiles are negligible for  $r > 3$ .

We assume that the electron temperature,  $T_e$ , is constant in the inner flow. For most of spectra presented in this paper, we assume  $kT_e = 5$  keV, at which the BMC dominates over thermal effects (e.g., Blandford & Payne 1981a; Ebisawa et al. 1996).

In all simulations, seed photons come from blackbody emission of the Keplerian disc. Except for a model with the free-falling plasma overlapping with the disc (Section 3.6), we take into account emission from the area of the disc between  $r_{\text{tr}}$  and  $r_{\text{out}} = 100$ . The latter value is chosen because illumination of the inner cloud by emission from  $r > 100$  is negligible and thus an increase of  $r_{\text{out}}$  above 100 does not affect resulting BMC spectra. The thermal emission of the disc is modelled as in N05; namely, the point of emission of each photon is generated according to the radial distribution of the disc emissivity (Page & Thorne 1974) and the

photon energy (in the disc local rest frame) is generated from the blackbody distribution corresponding to the local temperature. Note that the radial emissivity (and hence the temperature profile) is derived with the boundary condition of the vanishing stress at  $r_{\text{ms}}$  (where  $r_{\text{ms}}$  is the radius of the marginally stable orbit), valid for a disc extending down to  $\leq r_{\text{ms}}$ . In models with the disc truncated at  $r_{\text{tr}} > r_{\text{ms}}$ , deviations from this radial dependence may occur, e.g., a decrease of the energy emitted by the disc due to a lower amount of mechanical energy transported outward. On the other hand, magnetic stresses may be important near the  $r_{\text{ms}}$ , modifying somewhat the above boundary condition and thus the emissivity profile (e.g., Merloni & Fabian 2003 and references therein). However, quantitative description of these effects would require hydrodynamical models of the disc and its transition into the free-falling plasma, which is beyond the scope of this paper.

Photons illuminating the region of the free-fall are traced through their consecutive scatterings until they are captured by the black hole, hit the disc, or escape the flow. Compton reflection and reprocessing by the disc are not taken into account. The spectra presented here correspond to the escaping photons as seen by a distant observer and are angle-averaged. Simulation of Compton scattering is performed, in the plasma rest frame, according to the procedure described in Górecki & Wilczewski (1984). In modelling Comptonization spectra, we consider two cases, one with photon trajectories approximated by straight lines, and the other with a full GR description of photon motion, hereafter referred to as the flat and GR models, respectively.

Our GR model fully follows the procedure described in N05, involving solution of equations of photon motion in a curved space-time. The optical depth along a photon trajectory in a radially inflowing plasma is given by,

$$d\tau = \hat{n} \frac{\sigma(E_{\text{rest}})}{\sigma_{\text{T}}} \gamma \left( \frac{\Delta\Sigma}{A} \right)^{1/2} \left( \frac{d\hat{t}}{d\zeta} - \frac{A^{1/2}\beta^r}{\Delta} \frac{dr}{d\zeta} \right) d\zeta. \quad (7)$$

This is derived, similarly as in N05, from the elementary expression for the probability of scattering in the plasma rest frame,  $d\tau = n\sigma dl$ , where  $dl$  is the length of photon trajectory measured in the plasma rest frame. In the above equation,  $\zeta$  is an affine parameter,  $\sigma$  is the Klein-Nishina cross-section averaged over the Maxwellian distribution of electron velocities [see eq. (8) in Górecki & Wilczewski (1984)] and  $E_{\text{rest}}$  is photon energy in the plasma rest frame (the energy is affected by both the gravitational shift and Doppler shift related to the free-fall velocity). Note that increase of the optical depth in equation (7) is written in terms of the increase of Boyer-Lindquist coordinates (which describe motion relative to a distant observer) along the photon trajectory; the derivatives  $dr/d\zeta$  and  $d\hat{t}/d\zeta$  are determined by equations of motion, see eq. (8) in N05.

On the other hand, photon trajectories in the flat model are approximated by straight lines and the optical depth has the form obtained from equation (7) for  $r \gg 1$ ,

$$d\tau = n\sigma(E_{\text{rest}})\gamma(1 - \beta^r \cos\phi_r) dl', \quad (8)$$

where  $\phi_r$  is the angle between the outward radial direction and the direction of photon motion in the static frame and  $dl'$  is the distance measured by a static observer (in the flat model, reference frames of static and distant observers are equivalent). Note that in our derivation of  $d\tau$ , basing

on the probability of interaction in the plasma rest frame, the kinematic term,  $\gamma(1 - \beta^r \cos\phi_r)$  (e.g., Blumenthal & Gould 1971; Weaver 1976), results from transformation of the length of a photon path between the plasma rest frame and the frame of a static observer. This term has to be taken into account in Monte Carlo simulations of relativistic Comptonization (e.g., Pozdnyakov, Sobol' & Sunyaev 1983; Górecki & Wilczewski 1984). Equation (8) can be also derived from the probability of interaction written in terms of quantities defined in the frame of a static observer (denoted by an apostrophe),  $d\tau = \alpha' dl'$ , where  $\alpha' = \sigma'(E')n'$ , taking into account the Lorentz invariance of  $E\alpha$  (e.g., Rybicki & Lightman 1979, section 4.9).

All the remaining assumptions in the flat model are the same as in the GR model, in particular, capture of photons crossing the event horizon (assumed in the flat model at  $r_{\text{hor}} = 2$  for  $a = 0$ ). Obviously, our flat model is not self-consistent. We consider it in order to illustrate the crucial impact of space-time curvature on emerging spectra. Also, a number of previous studies neglected the curvature of the space-time and our flat model allows to directly compare these previous results with our Monte Carlo simulations.

We emphasize that an oversimplified method of integrating the optical depth along photon trajectories, neglecting both the gravitational and kinematic effects, have been used in some studies of BMC. See, e.g., eq. (2) in LT99 for the radial Thomson optical depth, which follows directly from  $d\tau = \sigma_{\text{T}} n dR$ , with  $n$  being the rest density and  $\sigma_{\text{T}}$  giving the probability of interaction with electron at rest but  $dR$  being the change of the Schwarzschild radial coordinate.

In order to illustrate the significance of the relativistic terms in equation (7), we consider now the Thomson optical depth for a *radial* trajectory in the Schwarzschild metric. For  $a = 0$ ,  $T_e = 0$  and null angular momentum of a photon, equation (7) yields

$$d\tau = \hat{n}\gamma(1 \pm \beta^r)(1 - 2/r)^{-1/2} dr. \quad (9)$$

The last two terms give the proper length in the Schwarzschild geometry,  $g_{rr}^{1/2} dr$ , where  $g_{rr} = (1 - 2/r)^{-1}$ , and  $\gamma(1 \pm \beta^r)$  gives the Lorentz transformation from the plasma rest frame; specifically,  $\gamma\hat{n}$  gives the density of electrons in the frame of a static observer and  $\sigma_{\text{T}}(1 \pm \beta^r)$  gives the probability of interaction with a beam of electrons moving with the velocity  $\beta^r$  (e.g., Weaver 1976). For the free-fall velocity field,  $\beta^r = -(2/r)^{1/2}$ , and then equation (9) yields

$$d\tau = \frac{\hat{n} dr}{1 \pm (2/r)^{1/2}}. \quad (10)$$

The upper and lower sign in equations (9) and (10) corresponds to ingoing ( $dr/d\zeta < 0$ ) and outgoing photons, respectively. (Note that the optical depth remains finite for ingoing photons at the event horizon.) The non-relativistic (for, in particular,  $\beta^r \ll 1$ ) approach,  $d\tau = \hat{n} dr$ , yields roughly two times higher optical depth than our equation (10) for ingoing photons, while for photons escaping from the vicinity of the event horizon, it underestimates  $\tau$  by a factor of a few. Equation (10) implies a significant decrease of the probability of escape from the innermost region of a free-falling flow with respect to photon transfer in a static plasma with the same rest density.

Monte Carlo simulations of BMC for both flat and GR (with  $a = 0$ ) models were presented in LT99. In both cases,

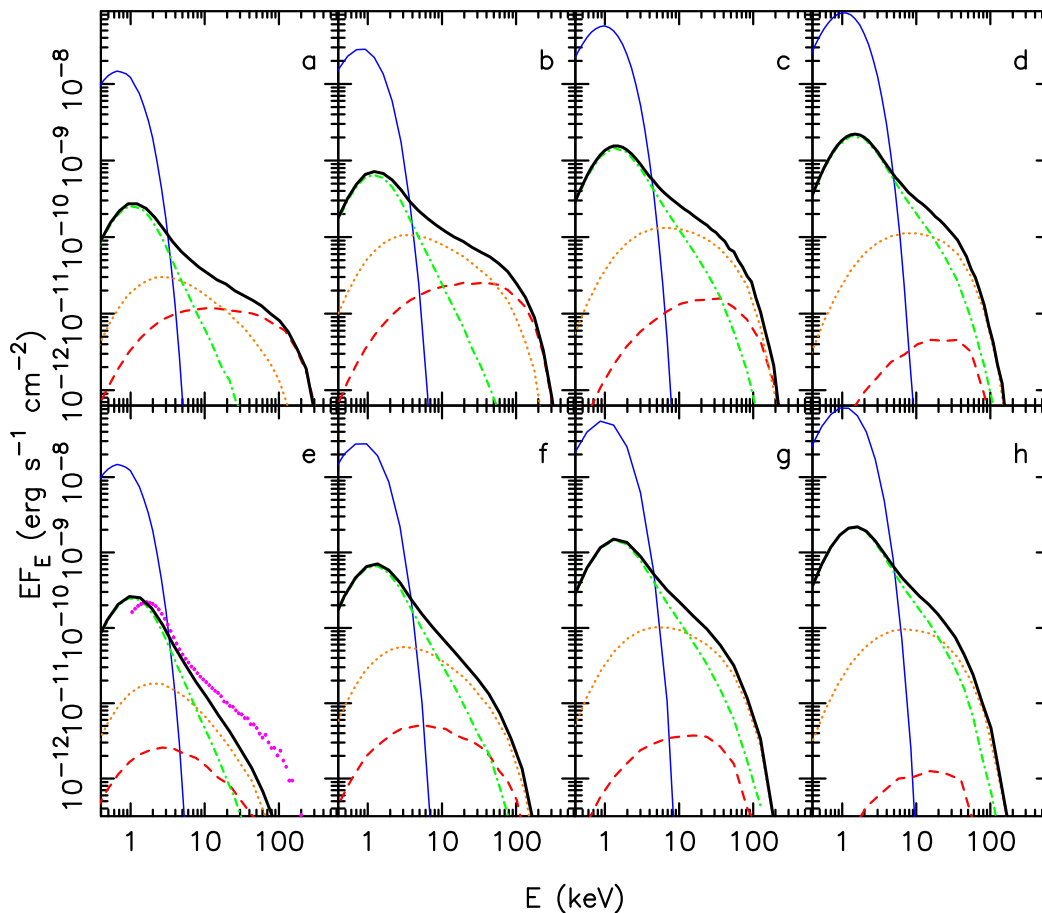


**Figure 1.** Emerging spectra for models with a Keplerian disc outside  $r_{\text{tr}} = 20$  and a spherical, free-falling, cold ( $kT_e = 5$  keV) inflow inside  $r_{\text{tr}}$ . The unscattered part of the blackbody disc emission and the Comptonization spectra are shown by the thin (blue online) and heavy (black) solid curves, respectively. All spectra are angle-averaged and correspond to a black hole with  $M = 10M_{\odot}$  at a distance of  $d = 5$  kpc. The accretion rate is  $\dot{m} = 2, 4, 8$  and  $12$  from left to right. The top panels show spectra for the flat model, and the bottom panels are for the GR model with a non-rotating black hole. The dashed (red online), dotted (orange online) and dot-dashed (green online) curves show contribution from photons for which the smallest scattering radius is within  $r = 2\text{--}5, 5\text{--}8,$  and  $8\text{--}20$ , respectively. The (magenta online) points in (e) show the spectrum for  $\dot{m} = 2$  and  $kT_e = 5$  keV obtained by LT99 in their GR model.

the assumptions underlying their simulations are similar as in this paper (they assume different spatial distribution of the source of soft photons, which, however, affects only slightly the BMC spectrum, see Section 3.6). However, both their flat and GR models appear to neglect the dependence of the probability of interaction on the angle between photon momentum and the direction of the bulk motion. As we discuss above, this may result in strongly overestimated emission from the inner region. In Section 3.5 below, we indicate this effect as a possible explanation for discrepancies between results of our model and LT99 at high accretion rates. On the other hand, the GR model developed in LT99 takes into account the GR term,  $g_{rr}^{1/2}$ , for the proper length in calculation of  $\tau$  (L. Titarchuk, personal communication).

In order to thoroughly test our method and results, we have also developed an independent model for Comptonization in the Schwarzschild metric (Niedźwiecki & Sitarek, in preparation), which involves a much simpler description of GR effects than our Kerr metric model. We have obtained results fully consistent with these presented here for  $a = 10^{-3}$ , in particular those where we encountered some discrepancies with previous studies.

### 3 RESULTS

Spectra emerging in models with  $r_{\text{tr}} = 20$ ,  $kT_e = 5$  keV,  $M = 10M_{\odot}$  and various accretion rates are shown in Fig. 1(a–d) for the flat model and in Fig. 1(e–h) for the GR model with a non-rotating black hole. We also show contributions from photons scattered in various parts of the inner flow.

#### 3.1 The cutoff energy in the flat model

In the flat model, the cutoff energy decreases with increasing  $\dot{m}$ , starting from  $\sim 100$  keV at low accretion rates to a few tens of keV at  $\dot{m} \gtrsim 10$ . As illustrated in Fig. 1(a–d), this decrease of the cutoff energy is primarily related to the diminishing contribution of radiation emerging from inner parts of the flow. In the flat model, the innermost parts generate radiation extending to highest energies. However, the optical depth for photons moving outward in the innermost region is typically a few times higher than for photons moving inward, see Section 2. As a result, photons at high accretion rates are trapped in the inner flow and carried under the event horizon. Such trapping has been considered,

e.g., by Begelman (1979) and Payne & Blandford (1981), who defined the trapping radius,  $r_{\text{trap}} \sim \dot{m}$ , as the distance at which the diffusion velocity equals the flow velocity.

An increase of  $\dot{m}$  results then in an increase of the trapping radius and depletion of increasing number of photons from the high-energy part of the spectrum. Moreover, photons that diffusively escape from the region inside  $r_{\text{trap}}$  lose a significant fraction of their energy in scatterings, compare the dashed and the heavy solid curves in Fig. 1(d). In the flat model, the position of the trapping radius is crucial for the dependence of the cutoff energy on the accretion rate.

We note that the formula derived in Titarchuk et al. (1997) for BMC in flat space-time,  $E_{\text{cut}} = [4/\dot{m} + (4/3)(v^r/c)^2]m_e c^2$  [note that the form of the second term in their eq. (9) is valid only for a plasma with  $v^r = -(2/r)^{1/2}c$ ; here we use a more general form which can be derived from Appendix D of their paper], predicts the cutoff energies a few times higher than these found in our simulations even when setting  $v^r = 0$ . The cause for that discrepancy is that their analysis ignores photon trapping and is based on the assumption that the cutoff occurs at photon energies for which energy gains are balanced by Compton recoil. We find that although the average increase of photon energy in a scattering indeed increases with decreasing  $\dot{m}$  (as a lower density results in a higher average velocity difference between scatterings), the above formula strongly overestimates the cutoff energy. Even at low accretion rates,  $\dot{m} < 4$ , for which trapping is not important, the formula is not consistent with our results, yielding unrealistic values of  $E_{\text{cut}} > 500$  keV, regardless of the value of the radial velocity.

### 3.2 The cutoff energy including space-time curvature

The spectra in the Schwarzschild GR model are cut off below 100 keV for all values of the  $\dot{m}$ , see Fig. 1(e–h). Thus, bending of photon trajectories strongly diminishes the contribution from the innermost region with respect to the flat model. This is due to several effects.

As explained below, basic properties of photon motion imply that for  $a = 0$  all photons escaping the flow from  $r \leq 5$  (i.e., avoiding crossing the horizon) are strongly redshifted as seen by a distant observer. Therefore, the emission from the  $r = 2$ –5 region contributes negligibly to the overall spectrum in the GR model with  $\dot{m} = 2$ , in spite of the trapping surface being very close to the event horizon, whereas this region gives a major contribution to the 20–200 keV spectrum in the corresponding flat model, see Figs. 1(a), (e).

The observed photon energy,  $E_{\text{inf}}$ , is related to the energy in the plasma rest frame,  $E_{\text{rest}}$ , by

$$E_{\text{inf}} = (1 - 2/r)^{1/2} \gamma (1 - \beta^r \cos \Phi_r) E_{\text{rest}}, \quad (11)$$

where  $\Phi_r$  is the angle between the inward radial direction and the photon direction in the plasma rest frame. Taking into account that the Lorentz factor for  $\beta^r = -(2/r)^{1/2}$  reduces with the gravitational redshift,  $(1 - 2/r)^{1/2}$  (i.e., their product is unity), we obtain,

$$E_{\text{inf}} = [1 + (2/r)^{1/2} \cos \Phi_r] E_{\text{rest}}, \quad (12)$$

which implies that only photons emitted inward in the plasma rest frame ( $\Phi_r < \pi/2$ ) are observed as blueshifted.

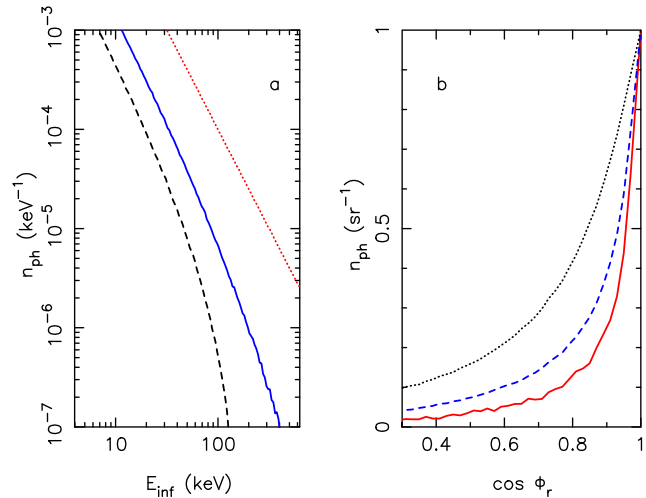


**Figure 2.** (a) The dashed (black online) and solid (blue online) curves show the angle-averaged spectra of photons at infinity that scatter at  $3.5R_g$  in the Schwarzschild and extreme Kerr geometry, respectively, off electrons with the free-fall velocity ( $v^r \approx -0.75c$  in both cases). The incident photons, with the power-law spectrum shown by the dotted (red online) line, move in the inward radial direction. (b) The angular distribution of photons in the local rest frame scattered within the inner  $5R_g$  for  $\dot{m} = 4$ . The number of photons per unit solid angle is given as a function of the angle of the photon direction before scattering with respect to the radial direction ( $\cos \Phi_r = 1$  corresponds to the inward direction). The dashed (blue online) and solid (red online) curves show photons with the initial energy corresponding to  $E_{\text{inf}} < 40$  keV and  $> 40$  keV, respectively, in the Schwarzschild GR model. The dotted (black) curve is for photons with  $E_{\text{inf}} > 40$  keV in the flat model. The curves are normalized to unity at  $\cos \Phi_r = 1$ .

On the other hand, the half-angle of the cone of avoidance, as defined in Chandrasekhar (1983),

$$\tan \Phi = (r/2 - 1)^{1/2} (r/3 - 1)^{-1} (r/6 + 1)^{-1/2}, \quad (13)$$

corresponds to  $\Phi_r = \pi/2$  [for which the aberration of light gives  $\tan \Phi = 1/(\gamma|\beta^r|)$ ] at  $r = 5.2$ . Then, all photons escaping from  $r < 5.2$  must be emitted backward and thus they have  $E_{\text{inf}}/E_{\text{rest}} < 1$ . The above constraint is valid for  $a = 0$ . For  $a = 0.998$ , such an effective redshift of all escaping photons is restricted only to emission from  $r < 2$ . Note that the solution of the GR radiative transfer equation by Papatthanassiou & Psaltis (2001) similarly indicates that, due to the space-time curvature, the innermost region contributes negligibly to the BMC spectrum.

Another reason for the inefficiency of BMC is that the free-fall velocity is relatively small in the region where most of high-energy emission is generated. In the GR model, the major contribution to the high-energy part of the spectrum comes from photons scattered within  $r = 5$ –8, where velocity is at most mildly relativistic,  $v^r \simeq 0.5$ – $0.7c$ .

Finally, we point out the importance of an additional effect, occurring for photons undergoing scattering in the Klein-Nishina regime, which severely reduces emission of hard X-rays. Namely, the highest energies are achieved by photons scattered toward the center, which then must be scattered off the inward direction to escape the flow. However, photons are preferentially scattered forward (and subsequently captured) at high energies. Then, photons which

significantly change direction in a scattering, so that they can escape, lose much of their energy to the recoil. Furthermore, the decline of the Klein-Nishina cross section makes scattering of high-energy photons less probable.

The dashed curve in Fig. 2(a) shows the spectrum at infinity from scattering at  $r = 3.5$  of radially incoming photons with a power-law spectrum. At  $<40$  keV, the flux of escaping radiation is over an order of magnitude lower than the illuminating flux due to capture of the scattered photons. At  $>40$  keV, the preference of forward scattering combined with the Compton recoil result in a sharp spectral cutoff.

Fig. 2(b) shows the angular distribution of photons undergoing scattering within inner  $5R_g$  at  $\dot{m} = 4$ . The incident photons are strongly concentrated along the inward radial direction, and this concentration increases with the increasing photon energy. This radiation anisotropy results in depletion of hard X-rays from the radiation leaving the innermost region, crucial for the spectrum. Note the related steepening above  $\sim 40$  keV of spectra shown by dashed curves in Figs. 1(e-f). On the other hand, the concentration of photons in the radial direction is less pronounced in the flat model and thus the above effect is less important.

### 3.3 The BMC luminosity

In all the models with  $r_{\text{tr}} = 20$ , the luminosity of the Comptonization component is  $<0.04$  of the total luminosity. This fraction drops to  $<0.01$  when the transition occurs at the marginally stable orbit,  $r_{\text{tr}} = 6$ . While the BMC component emerging from a spherically symmetric inner cloud is roughly isotropic, the flux from a flat disc observed at an inclination,  $i$  (with respect to the symmetry axis) decreases with increasing  $i$  as  $F(i) \propto \cos i$ . As a result, the relative flux in the BMC component from systems observed edge-on is higher, e.g.,  $\sim 0.1$  for  $\cos i = 0.1$ , than in the average spectra (presented in this paper).

For  $r_{\text{tr}} = 20$ ,  $\simeq 0.05$  of the photons emitted by the disc illuminate the free-fall region. The fraction of photons crossing the free-fall region that are scattered is 40 and 80 per cent for  $\dot{m} = 2$  and 12, respectively. Also, both the average number of scatterings and the energy transferred to photons increase with increasing  $\dot{m}$ . E.g., Comptonization increases the energy of photons by a factor of 1.9 and 4.3 for  $\dot{m} = 2$  and 12, respectively. However, an increase of  $\dot{m}$  also results in an increase of the trapping radius and a higher fraction of the photons being captured by the black hole, e.g., 20 and 40 per cent at  $\dot{m} = 2$  and 12, respectively. Moreover, trapping affects primarily photons scattered at small  $r$ , which achieve the highest energies and carry a significant fraction of the total energy transferred to photons. Again for  $\dot{m} = 2$  and 12, 20 and 40 per cent of the photons that get captured carry 50 and 85 per cent, respectively, of the total power in scattered photons. The resulting conclusion is that the luminosity in the BMC component is generally lower than the (initial) luminosity in the blackbody photons irradiating the plasma.

### 3.4 Black hole spin

Both the radial velocity and density profile changes with varying  $a$  are negligible for the considered spherical free-falling plasma. A significant impact of the space-time metric

on BMC spectra arises only due to properties of photon trajectories in the vicinity of the event horizon. The number of photons escaping from the innermost region increases with the increasing  $a$  for other parameters unchanged. Furthermore, the escaping photons have slightly higher blueshifts at higher values of  $a$ . For example, in the case of  $a = 0.998$ , the maximum blueshift,  $E_{\text{inf}}/E_{\text{rest}} = 1.5$ , is obtained for photons escaping from  $3 < r < 8$ , while for  $a = 0$ , the maximum blueshift increases from 1 at  $r = 5.2$  to 1.3 at  $r = 8$ . Such differences in photon motion make the steepening of the high-energy part of the spectrum generated by scattering at  $r = 3.5$  in the extreme Kerr metric less pronounced than in the case of the Schwarzschild metric (Fig. 2a).

Fig. 3 compares observed spectra at  $a = 0$  and  $a = 0.998$  for the same accretion rates. In the case of illumination by the external disc, Fig. 3(a-c), Comptonization spectra depend very weakly on  $a$ . The strongest dependence might have been expected for low  $\dot{m}$ , for which photons scattered close to the event horizon are not trapped. For  $\dot{m} = 0.5$ , Fig. 3(a), the spectra in models with  $a = 0.998$  and  $a = 0$  are dominated above 15 keV by emission from  $r < 5$  and  $5 < r < 8$ , respectively. However, the related difference between these spectra is rather moderate; most noticeably, the cutoffs occur at  $\sim 30$  and  $\sim 50$  keV for  $a = 0$  and 0.998, respectively. Note also that for such low values of  $\dot{m}$ , the BMC process is very inefficient, yielding spectra with  $\Gamma \gtrsim 4$ . For  $\dot{m} \geq 4$ , the spectra are dominated by photons for which the last scattering takes place at relatively large values of  $r$ , where the differences between low and high  $a$  are small. This makes the black hole spin weakly important for the spectrum.

Strong gravity effects may affect dynamics of Compton scattering in the ergosphere of a rapidly rotating black hole (Piran & Shaham 1977). We find, however, that such effects are not important for the formation of BMC spectra due to strongly relativistic radial velocities. Ergospheric emission of a cold free-falling plasma is strongly collimated inward and it does not give any significant contribution to the observed spectrum. Thus, we confirm a conclusion of N05 that a quasi-Keplerian motion is needed to make radiative processes in the ergosphere important for spectral formation.

### 3.5 Spectral index

For all spectra, we determine the photon spectral index,  $\Gamma$ , in the 10–30 keV energy range. Below 10 keV, contribution from thermal Comptonization with  $kT_e = 5$  keV is important, and significant departures from a power-law occur in some models above 30 keV.

The values obtained by us for  $\dot{m} > 4$  in the Schwarzschild GR model and for  $\dot{m} > 10$  in the flat model agree with  $\Gamma = 3$  of the solution of the transfer equation in the diffusion approximation (e.g., Payne & Blandford 1981). At low accretion rates, spectra of the flat model are harder,  $\Gamma \simeq 2.6$  for  $\dot{m} \leq 4$ , due to the strong contribution from the innermost region. This appears to be due to neglecting terms  $\propto (v/c)^2$  in the transfer equation of Payne & Blandford (1981), which may significantly underestimate the change of energy of a photon scattered in a plasma with a relativistic velocity (Psaltis & Lamb 1997).

On the other hand, spectra at low accretion rates in the GR model are much softer,  $\Gamma \gtrsim 3.5$  for  $\dot{m} \leq 2$ . A steepening with decreasing  $\dot{m}$  also characterizes spectra obtained by

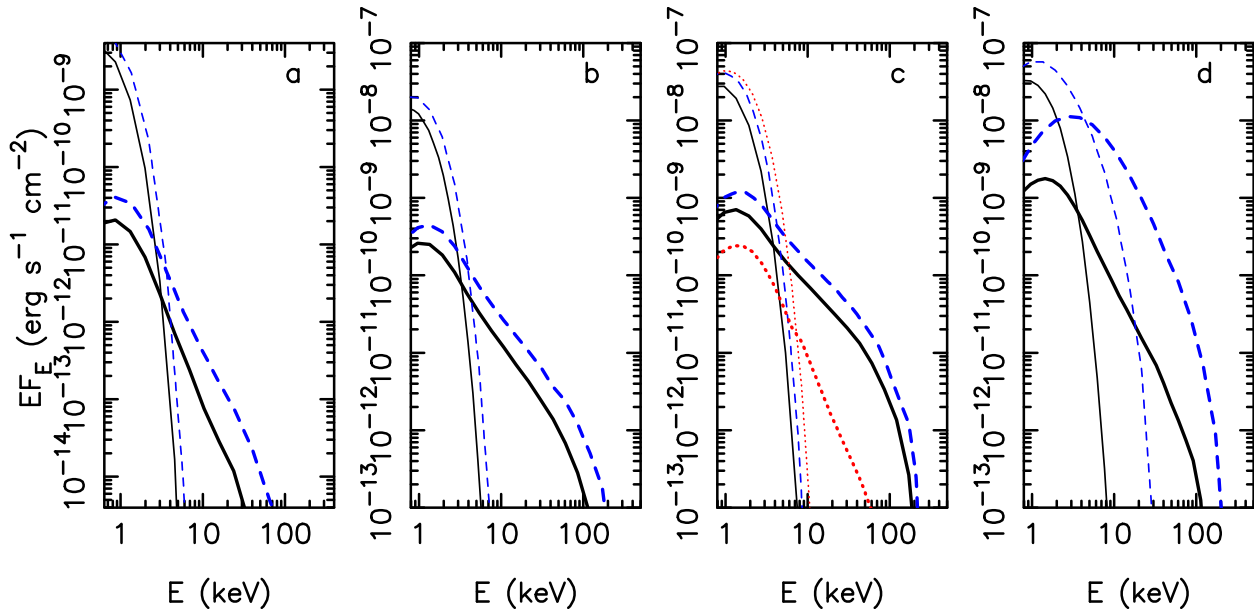


**Figure 3.** The solid and dashed (blue online) curves show spectra for the GR model for  $a = 0$  and  $a = 0.998$ , respectively. The thin and heavy curves show the emission from the thermal disc and from the BMC, respectively. The  $\dot{m} = 0.5$  (a), 2 (b), 4 (c), and  $r_{\text{tr}} = 20$ ,  $M = 10M_{\odot}$ ,  $kT_e = 5$  keV. The dotted (red online) curves in (c) are for the GR model with  $r_{\text{tr}} = 6$ ,  $\dot{m} = 4$  and  $a = 0$ . The spectra in (d) are for the model with the disc extending down to the event horizon described in Section 3.6, with  $\dot{m} = 4$  and  $r_{\text{ff}} = 20$ .

LT99 for their GR model with  $kT_e = 5$  keV (see table 2 in LT99). However, their spectra are harder than ours at any value of  $\dot{m}$ . At high accretion rates, the difference is moderate, e.g.,  $\Gamma = 2.8$  for  $\dot{m} = 7$  in LT99 vs.  $\Gamma = 3$  in our model, and we find that it could be accounted for by including the kinematic term in the scattering probability (see Section 2). Indeed, we obtain  $\Gamma = 2.8$  with that term neglected in equation (7). The same conclusion is valid for the flat model. Table 1 in LT99 gives  $\Gamma = 2$  for their flat model with  $\dot{m} = 7$  and  $kT_e = 5$  keV, while our calculations yield  $\Gamma = 2.7$  at this  $\dot{m}$ . However, we obtain similarly hard spectra,  $\Gamma = 2.2$  at  $\dot{m} = 4-8$ , by neglecting the kinematic term in equation (8), approximately accounting for the difference.

At low  $\dot{m}$ , the discrepancies between our models and those of LT99 become more significant, and we have found no explanation for them. In particular, we obtain  $\Gamma = 3.6$  for  $\dot{m} = 2$  whereas LT99 find  $\Gamma = 2.9$ . Both of those spectra are compared on Fig. 1(e). The (unphysical) modification of  $d\tau$  described above does not resolve this discrepancy.

Furthermore, LT99 conclude that the change of the size of the region containing free-falling plasma between  $r_{\text{tr}} = 6$  and 40 has a weak effect on the spectra. We find an opposite property, with the spectra softening significantly when  $r_{\text{tr}}$  drops below 10. For  $r_{\text{tr}}$  approaching 6 (at  $a = 0$ ), the spectra soften by at least  $\Delta\Gamma = 1$  with respect to those shown in Fig. 1, as illustrated by the lower dotted curve in Fig. 3(c). The reason for that is obvious; as shown in Fig. 1, a major part of the high energy emission is generated in the flow beyond  $6R_g$ . Then the Comptonized component becomes much weaker and softer if the flow shrinks to  $r_{\text{tr}} = 6$ .

### 3.6 Illumination patterns

We find that spatial distribution of the sources of seed photons on the surface of the outer disc does not change the

shape of the BMC spectrum. By replacing emission from the whole outer disc by emission from its inner edge (at  $r_{\text{tr}}$ ), we obtain very similar slopes and cutoffs of the BMC component. This is in agreement with previous studies based on the solution of the radiative transfer equation, e.g., Titarchuk et al. (1997) and Papathanassiou & Psaltis (2001).

On the other hand, the relative geometry of the disc and the free-fall plasma may be crucial for the normalization of the BMC emission with respect to the disc blackbody. The relatively low normalization found above (as measured by, e.g., the ratio of the  $EF_E$  of the BMC spectrum at the point of intersection with the disc blackbody to the  $EF_E$  at the peak of the disc spectrum) is due to the small solid angle subtended by the scattering plasma as seen by the outer disc. This effect was noted, e.g., by Borozdin et al. (1999), who proposed that an overlap between the free-fall plasma with the disc, resulting in a stronger illumination, is needed to explain certain observations of soft states of black-hole binaries by the BMC model. We note that there is indeed some observational evidence for the disc extending close to the horizon in some black-hole binaries, e.g., from thermal disc emission and relativistic Fe profiles (Zhang, Cui & Chen 1997; Miller et al. 2002).

Therefore, we consider a model with a Keplerian, blackbody-emitting, disc extending down to the minimum stable orbit. Below it, the disc material continues to flow to the horizon without dissipation (e.g., Cunningham 1975; Muchotrzeb-Czerny 1986). We assume that a spherical plasma surrounds the disc at radii  $r \leq r_{\text{ff}}$ , where a half of the accreting matter forms the geometrically thin disc and the remaining half accretes through the spherical free fall. Then, the density of the plasma is determined by equation (5) but with a half of the total  $\dot{m}$ . The disc emits blackbody photons down to  $r_{\text{ms}}$  ( $= 1.23$  and 6 for  $a = 0.998$  and 0, respectively), but below  $r_{\text{ff}}$ , the temperature profile

corresponds to a half of the total  $\dot{m}$ . The disc absorbs incident photons also below  $r_{\text{ms}}$  (as it remains optically thick at the accretion rates we consider here; Reynolds & Begelman 1997).

Fig. 3(d) shows the resulting spectra for a model with  $r_{\text{ff}} = 20$  and the (total)  $\dot{m} = 4$ . The BMC component contains now 6 and 18 per cent of the total luminosity for  $a = 0$  and 0.998, respectively. On the other hand, the spectra of this component are significantly softer (by  $\Delta\Gamma \approx 0.5$  for  $a = 0$ ) than in the corresponding (with  $\dot{m} = 2$ ) model with truncated disc.

For  $a = 0$ ,  $>70$  per cent of the energy dissipated in the disc is released at  $r > 20$ . Therefore, a disc truncated at  $r = 20$  has a similar luminosity as a disc extending down to  $r_{\text{ms}}$ . However, a significant fraction of soft photons emitted within the plasma is scattered in the latter case, which results in the fraction of disc photons that are Comptonized increasing to 10 per cent (from 3 per cent for a truncated disc with  $\dot{m} = 4$ ). A related increase of the peak of the BMC component at  $\sim 1.5$  keV (formed mostly by the first scattering order) by a factor of  $\sim 3$  is clearly seen by comparing the heavy solid curves in Figs. 3(c) and (d).

On the other hand, over 30 per cent of the scattered photons are absorbed by the part of the disc within the free-fall region. Moreover, this absorption affects mostly photons scattered in the inner region. In the corresponding model with a truncated disc, a significant fraction of photons forming the high-energy part of the spectrum gets scattered at  $r = 5\text{--}8$  inward but then escape (after passing the turning point in the  $r$ -motion), crossing the equatorial plane. In contrast, those photons are absorbed in the model with the overlapping disc. On the other hand, this effect is much less significant for photons at lower energies, typically formed at larger distances. Thus, the decreased contribution of high energy photons results in a softer spectrum, with  $\Gamma = 4.1$  vs.  $\Gamma = 3.6$  in the truncated disc model with the same electron density.

In the case of  $a = 0.998$ , the seed photons are very centrally concentrated, with over a half of the disc luminosity produced at  $r \leq 5$ . Thus, they have relatively high energies, of several keV. As a result, a power-law shape of the spectrum is achieved only in a narrow energy range of  $\sim 20\text{--}70$  keV. Absorption of photons with highest energies by the disc is significant in this case, as photon trajectories are strongly bent toward the equatorial plane at small  $r$  in the extreme Kerr metric. A resulting BMC spectrum is shown by the heavy dashed curve in Fig. 3(d).

In the overlap model, an increase of  $\dot{m}$  yields a decrease of the relative normalization of the BMC component for  $a = 0.998$ , e.g., its contribution to the total luminosity decreases from 18 to 10 per cent for  $\dot{m}$  changing from 4 to 24. For  $a = 0$ , this relative fraction remains approximately constant, at  $\sim 6$  per cent. The fact that the efficiency of the process does not increase with increasing  $\dot{m}$  is due to the increasing number of photons trapped at high  $\dot{m}$  (Section 3.3).

The value of  $r_{\text{ff}}$  is crucial for the normalization of these models. A high normalization of the BMC component with respect to the disc one may be achieved if a very dense, free-falling, plasma extends out to further distances than considered above. If an optically-thick free-fall plasma covers the disc surface up to  $r_{\text{ff}} \gtrsim 100$ , most of disc emission is Comptonized. We note that the BMC model makes some specific

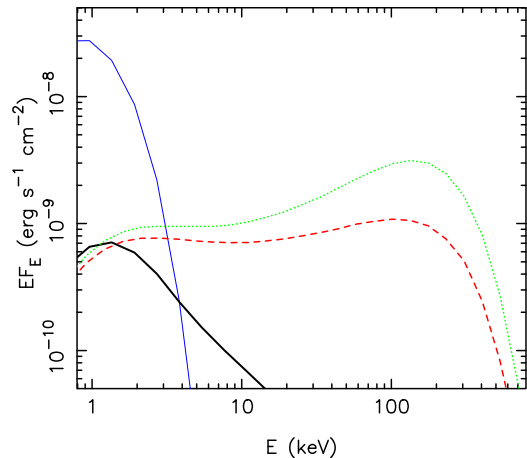


**Figure 4.** The dotted (green online) and dashed (red online) curves show Comptonization spectra from static and free-falling, respectively, plasmas at  $kT_e = 50$  keV. The heavy solid curve shows the spectrum from a free-falling plasma with  $kT_e = 5$  keV. The free-fall spectra are for  $\dot{m} = 4$  and the static plasma spectrum is for the same density distribution. All models have  $a = 0$ ,  $r_{\text{tr}} = 20$  and  $M = 10M_{\odot}$ . The thin (blue online) solid curve shows the blackbody disc emission (the same for all three models).

predictions for such scenario. Namely, the optical thickness of the free-fall plasma in the region within  $r \simeq 20\text{--}100$  is a few times lower than the optical thickness of the inner region,  $r \lesssim 20$ . Then, if the free-falling plasma is sufficiently dense to Comptonize most of disc emission from  $r \gtrsim 20$ , almost all of the total emission from the inner region will be trapped. Then, any relativistic signals from the innermost region, including relativistic fluorescent lines or high-frequency QPOs (assuming their relation to Keplerian frequencies), would not be observable. Furthermore, the BMC photons observed by a distant observer would come from scatterings at large  $r$  in a plasma with subrelativistic velocities. Then, spectrum would be precisely approximated by the flat model, i.e., would have  $\Gamma = 3$ .

LT99 argue that illumination of the central region can significantly increase if the surrounding disc is geometrically thick. They approximate this effect by emission from the inner edge of the disc at  $6R_g$ . However, emission from the surface of the disc is not shown in that paper, and thus the actual normalization is uncertain.

Summarizing this Section, we confirm that the relative normalization increase significantly when the source of seed photons is within the free-fall region. On the other hand, we find that then the BMC spectrum component becomes significantly softer than in corresponding models without overlap.

### 3.7 BMC vs. thermal Comptonization

Fig. 4 compares a BMC spectrum with spectra for semi-relativistic thermal Comptonization. For  $kT_e \gtrsim 10$  keV, thermal Comptonization completely dominates formation of spectra and the role of bulk motion is negligible (see also Jaroszyński 2001).

Fig. 4 also compares spectra from thermal Comptonization between static and free-falling plasmas with the same

rest density distributions. The major impact of the free fall on formation of thermal Comptonization spectra is by trapping photons in optically thick regions of inflowing plasma, making a Wien bump much less pronounced (which effect has been studied by Colpi 1988).

#### 4 DISCUSSION AND CONCLUSIONS

We have examined formation of spectra emerging due to multiple scattering of photons in black-hole accretion flows with relativistic radial velocities. In agreement with previous studies, we find that this model gives rise to power-law spectra with the photon spectral index of  $\Gamma \approx 3$  at high  $\dot{m}$ , which soften to  $\Gamma > 3$  with decreasing  $\dot{m}$ . The BMC process cannot explain spectra with  $\Gamma < 3$ . At semi-relativistic temperatures, needed to obtain such hard spectra by thermal Comptonization, the BMC process contributes negligibly to the spectral formation.

We point out effects preventing this power-law from extending beyond  $\sim 100$  keV. The recoil effect, dominant at lower accretion rates in flat space-time, results in a cutoff around 100 keV. At higher accretion rates, trapping of photons reduces contribution of photons from innermost regions. In a curved space-time, bending of photon trajectories combined with an increased probability of forward scattering at high energies result in cutoffs at a few tens of keV even at low accretion rates.

We do not confirm claims of, e.g., Titarchuk et al. (1997) and LT99, that the power-law spectrum extends to  $\sim m_e c^2$ . We find that such high energies are achieved only by photons scattered toward the center at very small radii, which then do not contribute to observed spectra.

In models with illumination of the free-falling plasma by the surrounding disc, the normalization of the BMC spectral component with respect to the peak of the disc blackbody spectrum is very low, typically  $\lesssim 10^{-2}$ . If a likely flattening of the plasma were taken into account, this relative normalization would become even lower. Higher normalizations may be obtained in models involving a disc extending down within the free-falling plasma. In this case, the high normalization occurs together with soft BMC spectra,  $\Gamma \gtrsim 4$ , due to absorption of Comptonized photons with highest energies by the inner disc. The luminosity of the (very soft) BMC component comparable to the disc one can only be achieved in models with complete obscuration of the central region, implying then no observable relativistic signatures.

We find that rotation of the black hole has a minor effect on the shape BMC spectra. The rotation is only important for models with the disc extending close to the event horizon, as in this case the fraction of soft seed photons emitted in the innermost region increases with an increase of  $a$ .

The amplitudes and spectral indices of high energy tails in some observations of black-hole binaries are consistent with the BMC model for moderate accretion rates,  $\dot{m} \lesssim 2$ . E.g., according to table 1 in Borozdin et al. (1999), the 1997 March 24 observation of GRO J1655–40 is consistent with parameters corresponding to the external illumination, and observations of 1997 April 24 and 30 are consistent with the untruncated disc. However, as discussed in Section 1, determination of the position of the high-energy cutoff is crucial for the confirmation that those spectra may be explained

by the BMC model. As shown by Tomsick et al. (1999), the high-energy tail of this object extends to  $\sim 2$  MeV, i.e., much higher than that possible to obtain in this model. In general, the BMC model is unable to explain the high energy tails of black-hole binaries in the soft state, which have often been measured to extend to energies  $\gtrsim 500$  keV without any cutoff, and often have too high amplitudes and/or  $\Gamma < 3$  (see, e.g., Zdziarski & Gierliński 2004).

A very low normalization of the high-energy tail (with a poorly constrained high-energy cutoff) is often seen in the ultrasoft (i.e., strongly dominated by a disc blackbody, e.g., Gierliński & Done 2004) states of black-hole binaries, see fig. 8 in Zdziarski & Gierliński (2004). However, those tails appear rather hard, e.g., with  $\Gamma \sim 2$  in GRS 1915+105 (Zdziarski et al. 2001).

Finally, we caution that a commonly-used implementation of the BMC model, BMC in the X-ray data fitting code XSPEC, allows for an arbitrary normalization of the Comptonization tail, arbitrary value of the spectral index as well as it does not include any high-energy cutoff, in contrast to the theoretical results. Thus, satisfactory results of fitting X-ray data with this model cannot be automatically taken as showing a consistency between that model and the data.

#### ACKNOWLEDGEMENTS

We thank L. Titarchuk and Ph. Laurent for discussions, and Ph. Laurent for supplying his Monte Carlo results. This paper was supported through KBN grants 1P03D01827, 1P03D01128, 4T12E04727 and PBZ-KBN-054/P03/2001.

#### REFERENCES

- Bardeen J. M., Press W. H., Teukolsky S. A., 1972, *ApJ*, 178, 347
- Begelman M. C., 1979, *MNRAS*, 187, 237
- Blandford R. D., Payne D. G., 1981a, *MNRAS*, 194, 1033
- Blandford R. D., Payne D. G., 1981b, *MNRAS*, 194, 1041
- Blumenthal G. R., Gould R. J., 1970, *RvMP*, 42, 237
- Borozdin, K., et al. 1999, *ApJ*, 517, 367
- Chakrabarti S. N., Titarchuk L., 1995, *ApJ*, 455, 623
- Chandrasekhar, S., 1983, *The Mathematical Theory of Black Holes*. Oxford Univ. Press, Oxford
- Colpi M., 1988, *ApJ*, 326, 223
- Cunningham C. T., 1975, *ApJ*, 202, 788
- D’Amico F., Heindl W. A., Rothschild R. E., Gruber, D. E., 2001, *ApJ*, 547, L147
- Di Salvo T., et al., 2000, *ApJ*, 544, L119
- Di Salvo T., Robba N. R., Iaria R., Stella L., Burderi L., Israel G. L., 2001, *ApJ*, 554, 49
- Di Salvo T., et al., 2002, *A&A*, 386, 535
- Ebisawa K., Titarchuk L., Chakrabarti S., 1996, *PASJ*, 48, 59
- Farinelli R., Frontera F., Zdziarski A. A., Stella L., Zhang S. N., van der Klis M., Masetti N., Amati L., 2005, *A&A*, 434, 25
- Gierliński M., Done C., 2004, *MNRAS*, 347, 885
- Gierliński M., Zdziarski A. A., Poutanen J., Coppi P. S., Ebisawa K., Johnson N. W., 1999, *MNRAS*, 309, 496
- Górecki A., Wilczewski W., 1984, *Acta Astronomica*, 34, 141
- Grove J. E., Johnson W. N., Kroeger R. A., McNaron-Brown K., Skibo J. G., Philips B. F., 1998, *ApJ*, 500, 899
- Iaria R., Burderi L., Di Salvo T., La Barbera A., Robba N. R., 2001, *ApJ*, 547, 412
- Jaroszyński M., 2001, *Acta Astronomica*, 51, 91
- Laurent P., Titarchuk L., 1999, *ApJ*, 511, 289 (LT99)

- Laurent P., Titarchuk L., 2001, *ApJ*, 562, L67  
Magdziarz P., Zdziarski A. A., 1995, *MNRAS*, 273, 837  
McConnell M. L., et al., 2002, *ApJ*, 572, 984  
Merloni A., Fabian A. C., 2003, *MNRAS*, 342, 951  
Miller J. M., et al., 2002 *ApJ*, 570, L69  
Muchotrzeb-Czerny B., 1986, *Acta Astronomica*, 36, 1  
Niedźwiecki A., 2005, *MNRAS*, 356, 913 (N05)  
Page D. N., Thorne K. S., 1974, *ApJ*, 191, 499  
Papathanassiou H., Psaltis D., 2001, *MNRAS*, submitted  
(astro-ph/0011447)  
Payne D. G., Blandford R. D., 1981, *MNRAS*, 196, 781  
Piran T., Shaham J., 1977, *Physical Review D*, 16, 1615  
Pozdnyakov L. A., Sobol' I. M., Sunyaev R. A., 1983, *Ap. Space Phys. Rev.*, 2, 189  
Psaltis D., 2001, *ApJ*, 555, 786  
Psaltis D., Lamb F. K. 1997, *ApJ*, 488, 881  
Reynolds C. S., Begelman M. C., 1997, *ApJ*, 488, 109  
Rybicki G. B., Lightman A. L., 1979, *Radiative Processes in Astrophysics* (New York: Wiley)  
Shrader C., Titarchuk L., 1998, *ApJ*, 499, L31  
Shrader C., Titarchuk L., 1999, *ApJ*, 521, L121  
Titarchuk L., Mastichiadis A., Kylafis N. D., 1997, *ApJ*, 487, 834  
Titarchuk L., Zambias T., 1998, *ApJ*, 493, 863  
Tomsick J. A., Kaaret P., Kroeger R. A., Remillard R. A., 1999, *ApJ*, 512, 892  
Turolla R., Zane S., Titarchuk L., 2002, *ApJ*, 576, 349  
Ueda Y., et al., 2002, *ApJ*, 571, 918  
Weaver T. A., 1976, *PhRvA*, 13, 1563  
Zdziarski A. A., 2000, in P. C. H. Martens, S. Tsuruta & M. A. Weber, eds., *IAU Symp. 195, Highly Energetic Physical Processes and Mechanisms for Emission from Astrophysical Plasmas*. ASP, San Francisco, p. 153 (astro-ph/0001078)  
Zdziarski A. A., Gierliński M., 2004, *Progr. Theor. Phys. Suppl.*, 155, 99  
Zdziarski A. A., Grove J. E., Poutanen J., Rao A. R., Vadawale S. V., 2001, *ApJ*, 554, L45  
Zhang S. N., Cui W., Chen W., 1997, *ApJ*, 482, L155